Development and Field Testing of an Optimal Path Following ASV Controller for Marine Surveys

Kleio Baxevani, Grant E. Otto, Herbert G. Tanner, and Arthur C. Trembanis

***Abstract*— Marine autonomous vehicles deployed to conduct marine geophysical surveys are becoming an increasingly used asset in the commercial, academic, and defense industries. However, the ability to collect high-quality data from applicable sensors is directly related to the robustness of vehicle motion caused by environmental disturbances. In this paper we designed and integrated a new path following controller on an autonomous surface vehicle (ASV) that minimizes the linear and angular accelerations on the sensor's local frame. Simulation and experimental results verify reduction of vehicle motion, improvement in path following, and improvement in preliminary sonar data quality compared to that of the existing proportional-yaw path following controller.**

I. Introduction

Marine geophysical surveys are a critical first step in informing a wide variety of industries about the seafloor. For example, offshore construction (oil and gas, offshore wind, etc.) use them to make key decisions about offshore structures, scientists use them to explore new areas, support ocean models, and monitor geologic processes, and the maritime and defense sectors use them to make critical decisions about vessel navigation [1]–[3]. Many of these marine surveys are increasingly conducted utilizing ASVs to increase safety, decrease carbon footprint, and provide force multiplication for operational efficiency (Fig. 1).

In general, ASVs are smaller in size and weight than their crewed counterparts, which provides a clear logistic, financial, and environmental advantage. However, a key disadvantage to using a smaller vessel is its susceptibility to vessel motion caused by sea conditions and disturbances like waves and winds. Vessel motion, especially that of a high frequency or amplitude, is a leading factor in data quality degradation for virtually any hull-mounted marine geophysical survey, and it should be minimized to the fullest extent [4].

Counteracting the nuisance motion that an ASV exhibits can be done with expensive physical damping mechanisms, or rather using the dynamic behavior of its own path following controller. The latter can be easier to tackle than the former, both in terms of solution development as well as its implementation—the latter, for instance, would merely necessitate a software upgrade. This paper implements and demonstrates improved motion control of an ASV that can have a significant impact on its field performance and the quality of collected data, eliminating artifacts that cannot be easily removed in post-processing.

Fig. 1: Seafloor Systems Inc Echoboat 160 ASV can undertake missions such as environmental surveys, port security, and search and rescue operations.

Path following ASV controllers that ensure safety, promote energy efficiency, and yield high-quality sensor data are particularly advantageous in the conduct of marine geophysical surveys. Most of these ASVs are underactuated systems (only surge force and yaw moment is controllable out of the three degrees of freedom), and are subject to nonholonomic kinematic constraints [5]. Various methods have been explored for ASV control, including backstepping [6], [7], sliding mode control [8], [9], model predictive control [10], and fuzzy logic control [11]. Even though these approaches provide control schemes that enable ASVs to accurately track a desired trajectory by optimizing the angular velocity and consequently the yaw angle of the vessels, the optimality of the linear and angular accelerations is not guaranteed.

What is arguably more important than accurate path tracking in environmental surveys is reducing or ideally eliminating any oscillations of the sensor system and maintaining a constant forward speed. In this light, the contribution of this paper is the development, experimental implementation, and field testing of a new optimal path following controller that is capable of autonomously steering a small ASV along a desired path in sea state 2 conditions, while ensuring minimum linear and angular accelerations expressed on the local frame of the sensor. The field testing of the integrated system was performed by planning and executing a series

Baxevani, and Tanner are with the Department of Mechanical Engineering, University of Delaware. {kleiobax,btanner}@udel.edu.

Otto and Trembanis are with the School of Marine Science and Policy, University of Delaware. {gotto, art}@udel.edu.

Thanks to Wenxuan (Owen) Li for helping with the software integration and to Hunter Tipton and Kaitlyn McPherran for their assistance with field testing. Additional acknowledgements go to Roland Arsenault (University of New Hampshire - Center for Coastal Ocean Mapping), Marcos Berrera (Seafloor Systems) and Chelsea Fairbank (SBG Systems) for their multifaceted support.

of straight-line paths similar to that of a typical marine geophysical survey. The reported path following controller is particularly effective for vehicles executing surveys with sensor payloads for which the performance (or the data quality), is negatively affected by irregular or sudden vehicle motion.

The rest of the paper is organised as follows. A brief overview of the system is provided in Section II followed by Section III which introduces the mathematical description of the vehicle and sensor payload kinematics. Section IV presents the main technical results of the paper. The performance of the controller is first evaluated using numerical simulations in Section V, and Section VI lays out the hardware and software tools employed for this integration, along with the field testing results. Finally, Section VII concludes the paper with a short overview and provides possible directions for future work.

II. Overview of the System

The architecture of the overall motion planning and sonar acquisition system is illustrated in Fig. 2 with the arrows in the block diagram indicating the information flow between the different modules of the system. The differently colored outlines indicate the particular subsystem that individual modules belong to.

The motion planning and control system, outlined in blue in Fig. 2, runs onboard the vessel and executes the mission plan dictated by the operator/user via the graphical interface (outlined in green). The system's path planner receives the task selected by the operator and designs a collection of Dubins' vehicle paths to complete the task. (The selection of Dubins' curves for path planning has been made by the designer of the interface provided; it can possibly be changed, but this was not within the scope of the study reported here.) The waypoints of this path are then exported to the graphical interface for visual display and to the path follower module. This project focuses on upgrades to the path follower module.

The path follower module starts by estimating the azimuth and the crosstrack error between the referenced trajectory given by the waypoints, and the current pose of the vehicle based on the odometry data coming from the IMU sensor. Then, using the azimuth and the crosstrack error, it computes the reference control input for the vessel. This control reference is expected to be in the form of linear and angular velocity. Our upgraded path following controller generates desired linear and angular accelerations instead, so an intermediate step of numerically integrating these reference commands to produce reference linear and angular speeds is introduced. Once the reference (or "command") linear and angular velocities are computed, they are fed to the low-level controller, which utilizes a unicycle model to steer the ASV to the next waypoint.

The data collection process is executed by the sonar acquisition system (outlined in red) in Fig. 2, which runs independently onboard the vessel. The geopose information of the ASV is provided by the INS sensor located on the vehicle and stored along with the sonar data to the designated computer of the sensor for post-processing purposes.

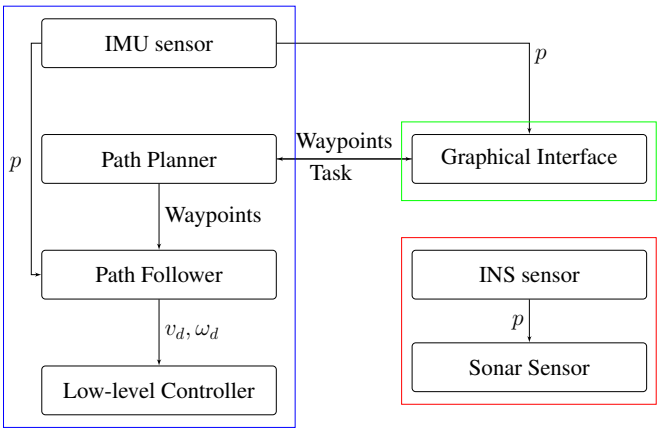

Fig. 2: Block diagram of the motion planning and sonar acquisition system architecture. *Blue*: The motion planning and control of the vehicle takes place onboard using odometry data given by the IMU sensor. *Green*: The graphical user interface runs on a groundstation desktop on-shore. *Red*: The sonar acquisition system records and stores data onboard using geopose information provided by the INS sensor.

III. Problem Formulation

A. Vehicle Kinematics

The kinematics of the Echoboat are assumed to be described by those of a unicycle with a dynamic extension. If (x, y) denotes the ASV's planar position (surge and sway displacement of the midpoint between the two propellers), θ its bearing (yaw angle of the normal to line segment connecting the propellers, relative to some fixed inertial frame $\{G\}$), and v and ω represent linear and angular velocity, respectively, then one writes

$$\dot{x} = v\cos\theta \tag{1a}$$
$$\dot{y} = v\sin\theta \tag{1b}$$
$$\dot{\theta} = \omega \tag{1c}$$
$$\dot{v} = a \tag{1d}$$
$$\dot{\omega} = \alpha \ , \tag{1e}$$

with the understanding that the linear and angular acceleration, a and α respectively, are considered the control inputs. The pose of the ASV can be denoted as $p = (x, y, \theta)^\intercal$. Let (χ, ψ) denote the coordinates of the ASV's sensor payload in $\{\mathcal{G}\}$; assuming that the sensor is placed somewhere along the longitudinal axis of symmetry of the vehicle and at a distance δ from the midpoint between the two propellers, these coordinates are expressed relative to the pose of the ASV as

$$\chi = x + \delta\cos\theta \tag{2a}$$
$$\psi = y + \delta\sin\theta \ , \tag{2b}$$

and because of (1), the dynamics of (2) take the form

$$\dot{\chi} = \dot{x} - \delta\,\sin\theta + \delta\,\dot{\theta}\cos\theta \tag{3a}$$
$$\dot{\psi} = \dot{y} + \delta\,\cos\theta + \delta\,\dot{\theta}\sin\theta \tag{3b}$$
$$\ddot{\chi} = a\cos\theta - v\,\omega\sin\theta - \delta\,\alpha\sin\theta - \delta\,\omega^2\cos\theta \tag{3c}$$
$$\ddot{\psi} = a\sin\theta + v\,\omega\,\cos\theta + \delta\,\alpha\cos\theta - \delta\,\omega^2\sin\theta\ . \tag{3d}$$

The objective now is to make (χ, ψ) follow desired straight line paths while exhibiting minimal acceleration, given that the latter has a detrimental effect on the quality of the data collected by the ASV sensor.

B. Sensor payload kinematics

This section outlines the design of a path following controller for (3), the objective of which is to minimize the linear and angular accelerations of the ASV as it steers it along desired line segments, fixed in $\{\mathcal{G}\}$. Consider the dynamics of the sensor position (χ, ψ) in the form of a double integrator:

$$\ddot{\chi} = u_\chi \tag{4a}$$
$$\ddot{\psi} = u_\psi\ , \tag{4b}$$

where u_χ and u_ψ are virtual control inputs which can be matched with the right hand side of (3c)–(3d) and expressed in matrix form in terms of the ASV's control inputs and velocities as

$$\begin{bmatrix} u_\chi \\ u_\psi \end{bmatrix} = \begin{bmatrix} \cos\theta & -\delta\sin\theta \\ \sin\theta & \delta\cos\theta \end{bmatrix} \begin{bmatrix} a \\ \alpha \end{bmatrix} - \begin{bmatrix} \sin\theta & \delta\cos\theta \\ -\cos\theta & \delta\sin\theta \end{bmatrix} \begin{bmatrix} v\,\omega \\ \omega^2 \end{bmatrix}\ . \tag{5}$$

To define the (path following) control specification, proceed as follows. Place a fixed frame $\{\mathcal{F}\}$ at the start point of the path that the vehicle is to follow, and orient the x axis of $\{\mathcal{F}\}$ along the desired direction of motion. If there are multiple paths (say, arranged parallel to each other, to realize some lawnmower-kind of area coverage), then each line segment i is associated with its own frame $\{\mathcal{F}_i\}$, attached at the point where the ASV is supposed to start traversing that path. The different line segments can then be sequenced, and as the ASV completes following one line segment, it is assumed that it switches to the next, replacing $\{\mathcal{F}_i\}$ with $\{\mathcal{F}_{i+1}\}$. To keep notation simple, we do not index $\{\mathcal{F}\}$; it is implicitly assumed that it corresponds to the "active" path segment. We will also assume for simplicity that all path segments are parallel to each other. This does not necessarily limit the applicability of the analysis that follows, since all the path segments are fixed relative to the inertial frame; it is just that one needs to keep track of the orientation of each segment and account for its fixed orientation offset when mapping between ASV, path segment $\{\mathcal{F}\}$, and inertial frames $\{\mathcal{G}\}$.

IV. Optimal Path Following ASV Control

Let (χ_F, ψ_F) denote the local (in $\{\mathcal{F}\}$) position coordinates of the ASV's sensor. The path tracking error can then be defined as $e \coloneqq \psi_F$. Given that $\{\mathcal{F}\}$ is fixed, the kinematics of (χ_F, ψ_F) inherits the double integrator structure of those of (4) and becomes:

$$\begin{bmatrix} \ddot{\chi}_F \\ \ddot{\psi}_F \end{bmatrix} = \begin{bmatrix} u_\chi \\ u_\psi \end{bmatrix}\ . \tag{6}$$

Now fully expand the state of (6) as $z = (\chi_F, \psi_F, \dot{\chi}_F, \dot{\psi}_F)^\intercal$ in order to define a linear system of the form

$$\begin{bmatrix} \dot{z}_1 \\ \dot{z}_2 \\ \dot{z}_3 \\ \dot{z}_4 \end{bmatrix} = \begin{bmatrix} 0 & 1 & 0 & 0 \\ 0 & 0 & 0 & 1 \\ 0 & 0 & 0 & 0 \\ 0 & 0 & 0 & 0 \end{bmatrix} \begin{bmatrix} z_1 \\ z_2 \\ z_3 \\ z_4 \end{bmatrix} - \begin{bmatrix} 0 & 0 \\ 0 & 0 \\ 1 & 0 \\ 0 & 1 \end{bmatrix} \begin{bmatrix} u_\chi \\ u_\psi \end{bmatrix} \tag{7a}$$

$$\eta = \begin{bmatrix} 0 & 1 & 0 & 0 \end{bmatrix} \begin{bmatrix} z_1 \\ z_2 \\ z_3 \\ z_4 \end{bmatrix}\ . \tag{7b}$$

It is known [12] that for a linear system like (7) the optimal feedback law that would regulate the output $\eta = z_2$ while minimizing the functional

$$J(z, \eta) \coloneqq \int_0^\infty \|z\|^2 + r\,w^2\,\mathrm{d}t\ , \tag{8}$$

for some tunable parameter $r > 0$ which expresses the cost of actuation, is of the form

$$u_\psi = -\frac{1}{r}\begin{bmatrix} 0 & 1 \end{bmatrix} P \begin{bmatrix} \psi_F \\ \dot{\psi}_F \end{bmatrix}\ , \tag{9}$$

where P is the solution of the algebraic Ricatti equation (ARE) associated with the (lower dimensional compared to (7)) system:

$$\begin{bmatrix} \dot{\psi}_F \\ \ddot{\psi}_F \end{bmatrix} = \begin{bmatrix} 0 & 1 \\ 0 & 0 \end{bmatrix} \begin{bmatrix} \psi_F \\ \dot{\psi}_F \end{bmatrix} - \begin{bmatrix} 0 \\ 1 \end{bmatrix} u_\psi \tag{10}$$

$$y = \begin{bmatrix} 0 & 1 \end{bmatrix} \begin{bmatrix} \psi_F \\ \dot{\psi}_F \end{bmatrix}\ . \tag{11}$$

The analytic solution for u_ψ is actually expressed as:

$$u_\psi = -\frac{\psi_F}{\sqrt{r}} - \frac{\dot{\psi}_F\sqrt{2}}{r^{1/4}} = -\frac{y_F + \delta\sin\theta}{\sqrt{r}} - \frac{(v\sin\theta + \delta\,\omega\cos\theta)\sqrt{2}}{r^{1/4}}\ . \tag{12}$$

For the χ dynamics, assume a proportional velocity controller $u_\chi = \frac{1}{r}(v_d - \dot{\psi}_\chi)$, which will regulate the speed of the ASV to a desired reference v_d along the path. (Once again, the choice of a fixed travel speed for the ASV is motivated by sensor data collection considerations.) Note that the local ψ_F coordinate measures the longitudinal displacement of the ASV along the desired path. It is therefore reasonable to simplify the closed-loop ψ_F dynamics to

$$u_\chi = \tfrac{1}{r}(v_d - v)\ ,$$

given that the sensor data of interest are those collected at steady state along path following and not during the transient

ASV motion phases as it switches between path segments $i.e.$ turns. The (u_χ, u_ψ) pair now defines the (virtual) control input for the dynamics of the ASV's sensor (7a). Without loss of generality, assume that the path segments' orientation is aligned with the x axis of the inertial frame $\{\mathcal{G}\}$. In such a case, the ASV's yaw angle θ will coincide with the orientation offset relative to the desired direction of motion along the path, and (5) will take the form

$$\begin{bmatrix} \frac{1}{r}(v_d - v) \\ u_\psi \end{bmatrix} = \begin{bmatrix} \cos\theta & -\delta\sin\theta \\ \sin\theta & \delta\cos\theta \end{bmatrix} \begin{bmatrix} a \\ \alpha \end{bmatrix} - \begin{bmatrix} \sin\theta & \delta\cos\theta \\ -\cos\theta & \delta\sin\theta \end{bmatrix} \begin{bmatrix} v\,\omega \\ \omega^2 \end{bmatrix},$$

which can be directly solved for the acceleration inputs of the ASV:

$$\begin{aligned} \begin{bmatrix} a \\ \alpha \end{bmatrix} &= \begin{bmatrix} \cos\theta & -\delta\sin\theta \\ \sin\theta & \delta\cos\theta \end{bmatrix}^{-1} \cdot \left(\begin{bmatrix} \frac{v_d - v}{r} \\ u_\phi \end{bmatrix} + \begin{bmatrix} \sin\theta & \delta\cos\theta \\ -\cos\theta & \delta\sin\theta \end{bmatrix} \begin{bmatrix} v\,\omega \\ \omega^2 \end{bmatrix} \right) \\ &= \begin{bmatrix} \frac{v_d - v}{r}\cos\theta + u_\psi \sin\theta + \delta\,\omega^2 \\ \frac{\frac{v_d - v}{r}\cos\theta\sin\theta - u_\psi\cos\theta^2 + v\,\omega\cos\theta}{\delta\cos\theta} \end{bmatrix}, \end{aligned}$$

where u_ψ is given in (12).

V. Numerical Validation

The numerical validation of the minimum acceleration path tracking controller is carried out first in the ASV dedicated simulation environment (Fig. 3). To this end, the controller was implemented into the Project11 backseat driver[1], which is an operational graphical user interface and simulator, combined with path planning tools built on the ROS framework [13]. In simulation, the parameters for the vehicle (e.g., size) were manually set to match as close as possible those of the Seafloor Echoboat 160 ASV. Although the controller was tuned during validation for this specific vehicle, the path following controller itself is designed to be applicable to a wide range of ASVs, the kinematics of which can be captured at some high-level using unicycle equations.

The numerical studies conducted aimed at evaluating the performance of the optimal path following controller using the standard Project11 proportional yaw controller as a benchmark. In the simulation scenario, the two controllers were tested on a two line segment survey of total length 38 meters. The simulated trajectories of the ASV following the survey paths using the two controllers are marked in Fig. 3. The simulation results indicate that the optimal path following controller is able to steer the vehicle and stabilize it along the straight line path after each turn relatively faster than the Project11 controller; this can be verified by the transient response specification metrics of Table I, and it is also visually observable in Fig. 3.

[1]https://github.com/CCOMJHC/project11

Transient Response Specifications		
Controller	Rise Time [s]	Settling Time [s]
Project11	1.0	1.9
Min acceleration	0.2	0.3

TABLE I: Transient time specifications of Project11 proportional yaw controller and the minimum acceleration controller. Rise time was measured as the time needed for the vehicle to have a cross track error less than 0.1%. Settling time was measured as the time needed for the cross track error of the vehicle to be in the [-0.02,0.02] interval and stay in that range.

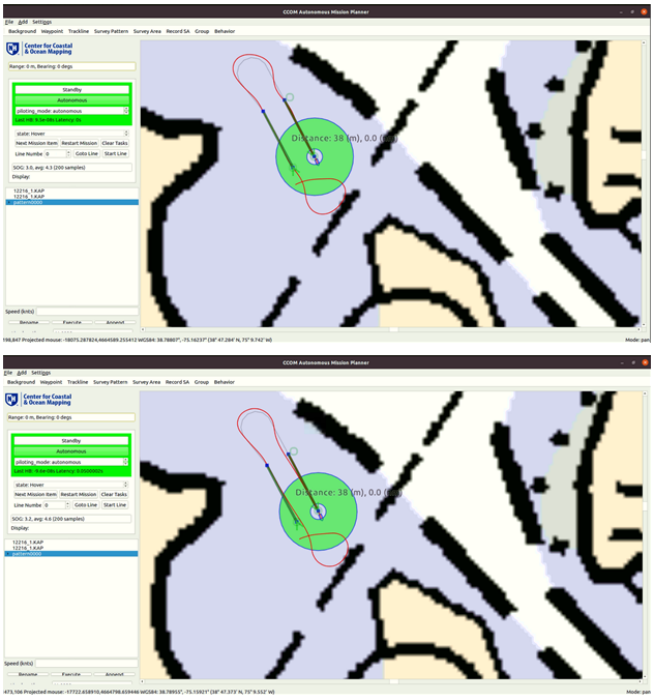

Fig. 3: Simulated environment of the UD's Hugh R. Sharp Campus boat basin. *Top*: Two-line survey conducted using the minimum acceleration path following controller. *Bottom*: Two-line survey conducted using Project11 proportional yaw controller.

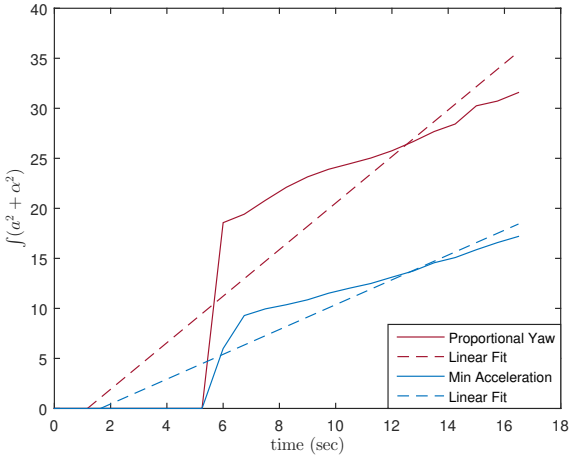

Fig. 4: Integral of the simulated linear and angular accelerations squared over time. The solid lines indicate the data points using the Project11 proportional-yaw controller (red) and the minimum acceleration controller (blue). The dashed lines denote the linear regression fit of the two datasets with red and blue respectively. The cumulative integral of the red curve is equal to 32.53, where the cumulative integral of the blue curve is equal to 17.47, showing an improvement of approximately 46%.

Figure 4 depicts the evolution of the acceleration (w^2 component) of the cost functional (8) over the course of one simulation test, for the two controllers. Figure 4 includes the average rate of increase for the components associated with the two controllers (captured by the slope of the dashed straight lines), indicating that the minimum acceleration path tracking controller effectively limits the rate of growth of the cost functional, as expected.

VI. Field Testing

The platform used to test the optimal path following controller was the Seafloor Systems Echoboat 160 ASV owned and operated by UD (Fig. 5). The Echoboat 160 is a versatile vehicle primarily used for shallow water mapping, and it is also a loosely-scaled proxy for larger vehicles used in open water environments. For this study, the vehicle was equipped with a Ping DSP 3DSS-DX interferometric sonar, georeferenced using navigation data from an SBG Ellipse-D3 dual GNSS antenna INS.

The field testing that assessed the implementation of the path following controller on the ASV was performed in the Delaware Bay in Lewes DE, USA. GPS and IMU data from a Pixhawk2 were used as control inputs to the path following control via MAVROS, which was previously integrated into Project11. The sonar data, with INS data injected in real-time, were logged and binned using Ping DSP's 3DSS Control software. The INS data were also redundantly logged for post processing using the SBG Data Logger tool. Although SBG provides a ROS driver for the Ellipse, we chose to use MAVROS for navigation input to the controller to maintain direct consistency with the wide range of ASV's where MAVROS is implemented.

Fig. 5: Sensor setup for the UD Seafloor Systems Echoboat 160 ASV comprised of the Ping DSP 3DSS-DX interferometric sonar and SBG Ellipse-D3 dual GNSS antenna INS.

Two field test surveys were performed in approximately sea state 2 conditions in the Delaware Bay, Lewes, DE; USA. Surveys were conducted within quick succession of each other (approximately 10 minutes) on the same day and during the same wave and tide conditions. The first survey was executed with the Project11 proportional yaw controller, and the second with the path following minimum acceleration controller. Bathymetry data were collected on the straight line paths of the surveys using the sonar and INS on the vehicle. The straight lines were oriented with a course of either 020 or 200 degrees, which were directly into or with (respectively) the wind and seas present at the time of testing.

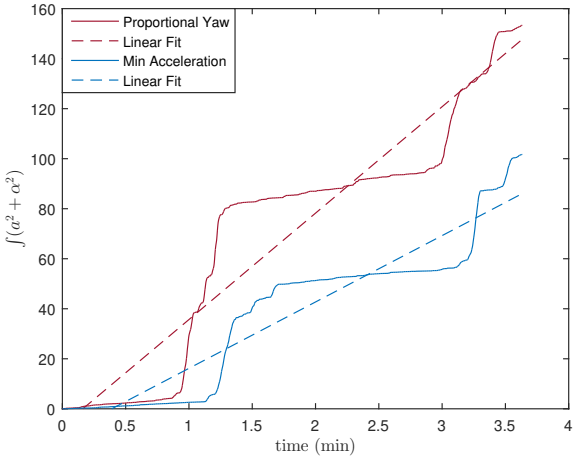

Fig. 6: Integral of the linear and angular accelerations, as provided by the INS sensor, squared over time. The solid lines correspond to the sensor data points using the Project11 proportional-yaw controller (red) and the minimum acceleration controller (blue). A linear regression model was then fit to the two datasets and is denoted with red and blue respectively. The cumulative integral of the red curve is equal to 101.71, where the cumulative integral of the blue curve is equal to 153.36, showing an improvement of approximately 33%.

Figure 6 depicts the evolution of the integral of the square of linear and angular accelerations over time (cf. Fig 4). The graph of the acceleration-squared integral of the optimal path following controller stays consistently below that of the one produced by the Project11 controller, matching the simulation results of Section V, illustrating the development of smaller accelerations and implying a more frugal utilization of onboard power. The difference is more visible during the phases where the ASV is turning (steep increases in the graphs of the two controllers), but is also present during the straight lines (flatter steps in the graphs of the two controllers) during which sonar data is conventionally collected.

Field testing produced sonar data which were processed using Qinertia (SBG) and SonarWiz (CTI) software, and are visually represented as ungridded soundings (Fig 7). The data were split into four parts, to highlight differences between the impacts of the Project11 proportional yaw controller (left column) and the minimum acceleration path following controller (right column) in head seas (travelling into the wind and waves, bottom row) and following seas (travelling with the wind and waves, top row). The data allow two preliminary observations for the optimal path following controller: (a) that the minimum-acceleration controller is more robust with respect to heading disturbances, and (b) that it also appears to outperform the benchmark controller in terms of transient response when settling on a path segment.

The former observation is supported by comparing the cyan rays emanating from left to right in the areas outlined by the solid line boxes in the upper half of Fig. 7: whereas on Fig. 7(1) there is a mix of rays of different orientations. Fig. 7(2) shows a more constant orientation, which is favorable for uniform, high quality data collection, whereas the

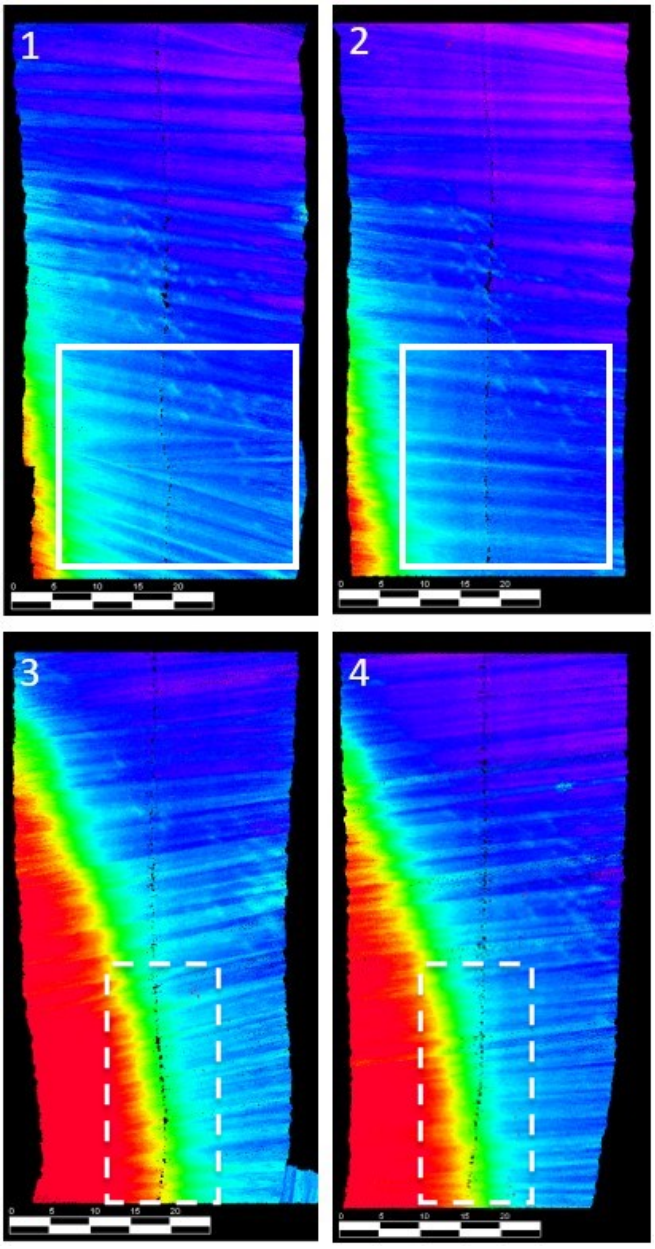

Fig. 7: Sonar bathymetry data. *1:* Project11 proportional yaw controller in following seas. *2:* Minimum acceleration controller in following seas. *3:* Project11 proportional yaw controller in head seas. *4:* Minimum acceleration controller in head seas.

effect in Fig. 7(1) is an artifact of the vehicle's meandering motion and introduces data contamination and less desirable sounding density. The difference between Fig. 7(1) and Fig. 7(2) is likely explained by an increased robustness to disturbances under the optimal path following controller.

The latter observation is supported by a comparison of the trail of black dots in the dashed boxes in the bottom half of Fig. 7: the curved initial bottom portion of the trail on Fig. 7(4) is indicative of an ASV that has more difficulty aligning with the path segment resulting in a larger gap in sensor coverage as evident by the larger black portion of Fig. 7(3). This could be attributed to the optimal path finding controller resulting in a higher order (compared to that of the benchmark's) closed-loop system that is capable of easier adjustment of its transient response.

Both hypotheses for the differences in the data quality between the left and right hand side of Fig. 7 are preliminary, given the quantity of data that supports them, but there is clear evidence to motivate further investigation.

VII. Conclusions and Future Work

This paper demonstrated the feasibility of integration and performance testing of a new minimum acceleration ASV motion controller in both simulation and field survey conditions, indicating its potential to increase efficiency and applicability of ASV operations in a dynamic ocean environment. Specifically, such a controller would allow an ASV to conduct marine surveys in a way that facilitates better coverage and improves the quality of acquired sonar data, without the utilization of expensive motion-damping hardware such as gyrostabilizers or keels. In addition, with control algorithms like the ones reported here, small ASVs can be deployed in environmental conditions typically reserved for larger vehicles. The broadened use case and increased operational efficiency of ASVs represent new opportunities for economic development and scientific discovery for a growing marine robotics industry.

References

[1] C. J. Brown, S. J. Smith, P. Lawton, and J. T. Anderson, "Benthic habitat mapping: A review of progress towards improved understanding of the spatial ecology of the seafloor using acoustic techniques," *Estuarine, Coastal and Shelf Science*, vol. 92, no. 3, pp. 502–520, 2011.

[2] J. R. Frost and L. D. Stone, "Review of Search Theory: Advances and Applications to Search and Rescue Decision Support," U.S. Department of Transportation, Washington, D.C., Tech. Rep. CG-D-15-01, 2001.

[3] B. B. Parker and L. C. Huff, "Modern under-keel clearance management," *The International Hydrographic Review*, vol. 75, no. 2, 2015.

[4] B. R. Calder and L. A. Mayer, "Automatic processing of high-rate, high-density multibeam echosounder data," *Geochemistry, Geophysics, Geosystems*, vol. 4, no. 6, 2003.

[5] T. I. Fossen, *Marine Control Systems: Guidance, Navigation and Control of Ships, Rigs and Underwater Vehicles*. Marine Cybernetics, 2002.

[6] J. Ghommam, F. Mnif, and N. Derbel, "Global stabilisation and tracking control of underactuated surface vessels," *IET control theory & applications*, vol. 4, no. 1, pp. 71–88, 2010.

[7] Y. Yang, J. Du, H. Liu, C. Guo, and A. Abraham, "A trajectory tracking robust controller of surface vessels with disturbance uncertainties," *IEEE Transactions on Control Systems Technology*, vol. 22, no. 4, pp. 1511–1518, 2013.

[8] Z. Sun, G. Zhang, J. Yang, and W. Zhang, "Research on the sliding mode control for underactuated surface vessels via parameter estimation," *Nonlinear Dynamics*, vol. 91, no. 2, pp. 1163–1175, 2018.

[9] N. Wang, X. Pan, and S.-F. Su, "Finite-time fault-tolerant trajectory tracking control of an autonomous surface vehicle," *Journal of the Franklin Institute*, vol. 357, no. 16, pp. 11 114–11 135, 2020.

[10] J. Gao, P. Wu, T. Li, and A. Proctor, "Optimization-based model reference adaptive control for dynamic positioning of a fully actuated underwater vehicle," *Nonlinear Dynamics*, vol. 87, no. 4, pp. 2611–2623, 2017.

[11] Y. Deng and X. Zhang, "Event-triggered composite adaptive fuzzy output-feedback control for path following of autonomous surface vessels," *IEEE Transactions on Fuzzy Systems*, vol. 29, no. 9, pp. 2701–2713, 2020.

[12] M. Athans and P. L. Falb, *Optimal control : An introduction to the theory and its applications*. McGraw-Hill New York ; Sydney, 1966.

[13] Stanford Artificial Intelligence Laboratory et al., "Robotic operating system." [Online]. Available: https://www.ros.org